Journal of Geophysical Research Atmospheres

Supporting Information for

Unrealized Global Temperature Increase: Implications of Current Uncertainties

Stephen E. Schwartz

Brookhaven National Laboratory, Upton NY USA

Contents of this file

Additional Supporting Information (File uploaded separately)

Introduction

The supporting information provides additional information, figures, and data in support of the main article. Numerical data corresponding to quantities shown in the figures in the main article and in this supporting information are presented in a multiple sheets of a single Excel file, ds01.xls.

Text S1. Time series of historical forcing

Time series of total forcing are required for the best-estimate forcing by anthropogenic aerosols and also for the high- and low-magnitude estimates of the aerosol forcing. The forcing time series denoted here "best estimate" is time series for total forcing for years 1750–2011 given in the Climate Scenario Tables of AR5 (Prather *et al*., 2013). The two additional forcing time series were determined by scaling the tabulated best-estimate aerosol forcing time series, denoted F_{aB}, by the uncertainty ranges for present (year-2011) forcing given in AR5 (Myhre *et al*., 2013, Figure 8.18), which gives as the best estimate of the present aerosol forcing -0.90 W m^{-2} with the 5–95% likelihood range of that forcing -0.09 to -1.88 W m^{-2}. The low-magnitude–bound aerosol forcing for year t was calculated from $F_{\mathrm{aB}}(t)$ as $F_{\mathrm{aL}} = F_{\mathrm{aB}}(t)\cdot(0.09/0.90)$, and similarly the upper-magnitude–bound aerosol forcing as $F_{\mathrm{aH}} = F_{\mathrm{aB}}(t)\cdot(1.88/0.90)$. These forcings were

added to the tabulated total forcing minus F_{aB}, to yield the time series for total forcing corresponding to the low- and high-magnitude aerosol forcings. The three time series are shown in Figure S1. Attention is called to the increasing difference among the several time series with increasing time as the magnitude of aerosol forcing increases.

Text S2. Impulse response functions and convolutions with historical forcings

For each of the values of S_{tr} in Table 1, corresponding to high, best-estimate, and low climate sensitivity, and respective values of S_{eq}, together with assumed short and long time constants of the climate system, τ_s and τ_l, an impulse response function was generated (Eq 4 of text) that gives the change in GMST at time $t + \delta t$ due to unit impulse forcing at time t. The impulse functions used here are shown in Figure S2 for τ_s = and τ_l equal to 7.5 and 500 yr, respectively. The important features are the rapid drop off at short time, the tail extending to long time, and the differences in values for the three sensitivity values determined here.

The time series for change in GMST obtained by convolution of the impulse response functions with the respective forcing functions are presented in Figure 1 of the text and are compared in Figure S3 to the temperature time series for the CMIP5 models presented by Flato *et al*. (2013).

Text S3.

For the present analysis the time derivative of forcing necessary for evaluation of Eq A.15 was calculated for the final 10 years of each of the forcing time series. The corrected and uncorrected sensitivity parameters inferred from the observed time series for ΔT and for the forcing time series corresponding to high-magnitude, best-estimate and low-magnitude aerosol forcing are presented in Table S1 for τ_s 5, 7.5 and 10 yr to examine sensitivity to τ_s, and in Figure 3. The unrealized increase in GMST, 0.03 to 0.12 K, is rather small relative to the observed increase in GMST between 1850–1900 and 2011, 0.78 K, although not negligible. The uncertainties on S_{tr} in Table S1 are due to the range of τ_s 5–10 yr and do not reflect other contributions to uncertainty.

Text S4. Relations between sensitivity and forcing

As shown in Figure 2*a* the values of transient sensitivity parameter unadjusted for unrealized warming, $S_{tr,u}$, determined by the scale adjustment procedure (Figure 1) are tightly correlated with the total forcing over the period 1850–1900 to 2011 over the range of forcing corresponding to the AR5 high and low estimates of aerosol forcing. Adjustment of the value of S_{tr} to account for unrealized warming (SI §S3) results in an increase in S_{tr} that is somewhat greater for higher values of sensitivity. The resulting empirical fit of S_{tr} to total forcing shown in Figure 2*a* thus exhibits a greater (negative) slope, -1.21, somewhat greater than the -1 slope corresponding to the inverse first-power relation between these quantities.

The fit of S_{tr} to total forcing in turn permits developing an empirical expression for the relation between S_{tr} and the aerosol forcing in year 2011 (relative to year 1750), the

quantity that is employed here in examination of climate system response to abrupt cessation of emissions. The resulting expression, shown in Figure 2*b*, is

$$S_{\mathrm{tr}} = 1.05(3.12 + 0.75F_{\mathrm{aer}})^{-1.214} . \qquad \text{(S4.1)}$$

As emphasized throughout this paper, the tight coupling between aerosol forcing and transient sensitivity, as reflected in Eq S4.1, greatly narrows the variable space that must be considered in examination of the change in GMST that would result from a change in forcing due to abrupt cessation of emissions, as examined here, or more generally in any examination of change in GMST to future change in forcing. The fit (Eq S4.1) also permits calculation of the dependence on aerosol forcing magnitude of the equilibrium sensitivity parameter S_{eq} and of the increase in GMST that would occur if response of the climate system were instantaneous $\Delta T_{\mathrm{inst,aer}}$ (Figure 2*b*) and permits graphing the maximum temperature increase and the time to reach maximum temperature increase following cessation of emissions versus aerosol forcing magnitude at time of cessation, SI §9, Figure S6.

Text S5. Carbon dioxide historical emissions

Determining the decay profile of atmospheric CO_2 that would result from a given impulse response function (IRF) involves convolution of the IRF with historical emissions prior to the cessation of emission, with the emissions function set to zero following cessation of emission. In view of the role of anthropogenic CO_2 as a climate forcing agent considerable effort has been directed to determining historical CO_2 emissions. Two broad classes of emissions are identified: 1) fossil fuel combustion and calcination of limestone associated with producing cement, and 2) land use change, net of deforestation minus afforestation, the decrease of standing carbon associated with deforestation mainly entering the atmosphere. The present analysis relies on determinations of CO_2 emissions summarized in AR5 (Ciais *et al*., 2013), and uses the updated tabulation of Le Quéré *et al*. (2015). Fossil fuel emissions are determined from energy consumption statistics and converted to emissions by fuel type (Marland and Rotty, 1984). Emissions from land use change are based on surveys of rates of deforestation and forestation (Houghton *et al*., 2012). According to Ciais *et al*., (2013) the 90% uncertainty range in annual global emissions is about ± 8%.

Text S6. Convolution of IRFs with CO_2 emissions

Several normalized decay profiles for atmospheric CO_2 presented in Figure 3 that would result from abrupt cessation of emissions were obtained by convolution of impulse response functions (IRFs, fraction of material emitted at time 0 remaining in atmosphere at time *t*) with emissions. The several IRFs examined, shown in Figure S4, exhibit substantial diversity, which is attributed to differing treatment of uptake of CO_2 into the ocean and the biosphere in the several models. Exponential decay curves (straight lines on the semi-logarithmic plot) are shown to lend perspective. The diversity in IRFs is reflected in the diversity of profiles of excess CO_2 versus time after cessation of emissions, Figure 3. Evident in all the IRFs examined is a decrease in the magnitude of

the slope (instantaneous fractional CO_2 drawdown rate) with increasing time subsequent to emission. This is a consequence of uptake of incremental CO_2 being initially largely into the upper ocean versus uptake at later time governed by much slower drawdown from the upper ocean to the deep ocean.

In calculating the CO_2 decay curves subsequent to cessation of emissions, historical emissions, terminated abruptly in 2006, were convolved with the several IRFs. The normalized decay profiles were evaluated from the CO_2 mixing ratio subsequent to cessation of emissions and expressed as $f_x(t)$, the fraction relative to the difference between the mixing ratio prior to cessation of emissions (2005) and the preindustrial mixing ratio (taken as 278 ppm), Eq (10), as a function of time t subsequent to cessation of emissions.

Text S7. Linear dependence of CO_2 forcing on mixing ratio

Forcing by incremental CO_2 is conventionally given as a logarithmic dependence on CO_2 mixing ratio (Myhre *et al*., 1998, 2013)

$$F([CO_2]) = \frac{F_{2\times}}{\ln 2} \ln \frac{[CO_2]}{[CO_2]^*} \tag{S7.1}$$

where $F_{2\times}$ is the forcing associated with doubling CO_2 and $[CO_2]^*$ is a reference mixing ratio. However for change in the mixing ratio of CO_2, $\Delta[CO_2] = [CO_2] - [CO_2]^*$, small compared to $[CO_2]^*$, to very good approximation the change in forcing is linear in $\Delta[CO_2]$,

$$\Delta F([\Delta CO_2]) = \frac{F_{2\times}}{\ln 2} \ln \frac{[CO_2]^* + \Delta[CO_2]}{[CO_2]^*} \approx \frac{F_{2\times}}{\ln 2} \frac{\Delta[CO_2]}{[CO_2]^*} = \beta \Delta[CO_2] \tag{S7.2}$$

where the linear forcing coefficient β is given by

$$\beta \equiv \frac{F_{2\times}}{\ln 2 \ [CO_2]^*} . \tag{S7.3}$$

This linear dependence is compared to the customary logarithmic expression for this forcing in Figure S5 for $\beta = 0.0151$ W m^{-2} ppm^{-1}, corresponding, for $F_{2\times} = 3.7$ W m^{-2}, to $[CO_2]^* = 355$ ppm. The close agreement between the two expressions supports the use of the linear expression in calculation of change in GMST following cessation of CO_2 emissions.

Text S8. Sensitivity of rate and magnitude of increase in GMST to climate system time constant

The sensitivity of the results shown in Figure 5 of the text to the choice of the time constant of the upper compartment of the climate system τ_s was examined (Figure S6) by evaluating ΔT for τ_s = 5, 7.5 (as in Figure 5) and 10 yr spanning the range of current

estimates (Gregory, 2000; Boucher *et al*., 2009; Held *et al*., 2010; Schwartz, 2012*a*; Geoffroy *et al*., 2013). For this comparison only the results for the case of high sensitivity and high aerosol forcing magnitude are shown, to better display the differences; the figure is on the same scale as Figure 5 permitting comparison with that figure. For any given value of adjustment time of excess CO_2, τ_{CO2}, the several curves corresponding to different τ_s are nested closely to each other, relative to the differences for different τ_{CO2} or different cases of aerosol forcing magnitude, Figure 5. For shorter τ_s the maximum value of ΔT is reached somewhat earlier and is slightly greater than for longer τ_s. However the important conclusion here is that the differences are negligible over the range of τ_s examined, demonstrating the insensitivity of the present results to choice of upper-compartment time constant.

Text S9. Maximum increase in GMST following cessation, and time of maximum increase

Change in global temperature (change in temperature of the upper compartment of the climate system) may be calculated for any temporal profile of forcing $F(t)$ by Equation 6 of the text, under assumption of steady state prior to t_{init} as

$$\Delta T(t) = \frac{S_{tr}}{\tau_s} e^{-t/\tau_s} \int_{t_{init}}^{t} e^{t'/\tau_s} F(t')dt' + \frac{S_{eq} - S_{tr}}{\tau_1} e^{-t/\tau_1} \int_{t_{init}}^{t} e^{t'/\tau_1} F(t')dt' ; \qquad (6)$$

where τ_s and τ_1 denote the short and long time constants of the climate system, ca 5–10 yr and 500 yr, respectively, and S_{tr} and S_{eq} denote the transient and equilibrium climate sensitivity parameters, respectively. For examination of the change in temperature subsequent to a change in forcing at time t_0 it is convenient to express the integral (6) as the sum of changes in temperature prior to and subsequent to t_0,

$$\Delta T(t) = \frac{S_{tr}}{\tau_s} e^{-t/\tau_s} \left\{ \int_{t_{init}}^{t_0} e^{t'/\tau_s} F(t')dt' + \int_{t_0}^{t} e^{t'/\tau_s} F(t')dt' \right\} + \frac{S_{eq} - S_{tr}}{\tau_1} e^{-t/\tau_1} \left\{ \int_{t_{init}}^{t_0} e^{t'/\tau_1} F(t')dt' + \int_{t_0}^{t} e^{t'/\tau_1} F(t')dt' \right\} . \qquad (S9.1)$$

Denoting $\Delta T(t_0)$ as the sum of the contributions from the transient and equilibrium responses,

$$\Delta T(t_0) = \Delta T_s(t_0) + \Delta T_1(t_0) \qquad (S9.2)$$

where

$$\Delta T_s(t_0) = \frac{S_{tr}}{\tau_s} e^{-t_0/\tau_s} \int_{t_{init}}^{t_0} e^{t'/\tau_s} F(t')dt' + \text{ and } \Delta T_1(t_0) = \frac{S_{eq} - S_{tr}}{\tau_1} e^{-t_0/\tau_1} \int_{t_{init}}^{t_0} e^{t'/\tau_1} F(t')dt' . \qquad (S9.3)$$

Here two cases are of particular interest. If forcing at time $t > t_0$ is abruptly set to zero, then

$$\Delta T(t) = e^{-(t-t_0)/\tau_s}\Delta T_s(t_0) + e^{-(t-t_0)/\tau_1}\Delta T_1(t_0);$$

That is, each of the two contributions to the perturbation in temperature at time t_0 decays with its own characteristic time constant. A second case of interest is when the forcing subsequent to time t_0 is maintained constant at its value at time t_0. In this situation the change in temperature from that at time t_0 is

$$\Delta T(t) - \Delta T(t_0) = [S_{tr}F(t_0) - \Delta T_s(t_0)][1 - e^{-(t-t_0)/\tau_s}] + [(S_{eq} - S_{tr})F(t_0) - \Delta T_1(t_0)][1 - e^{-(t-t_0)/\tau_1}] \quad \text{(S9.4)}$$

The first term in Eq S9.4 represents the unrealized increase in temperature from prior forcing shown in SI §S2 to be small; *cf*. Figure 5*a*. Neglecting that increase, the change in GMST relative to that at the time of cessation expressed as a function of the change in forcing relative to that at time t_0, $\Delta F(t'\text{-}t_0)$ is

$$\Delta T(t) - \Delta T(t_0) = \frac{S_{tr}}{\tau_s} e^{-(t-t_0)/\tau_s} \int_{t_0}^{t} e^{t'/\tau_s} \Delta F(t' - t_0) dt' + \frac{S_{eq} - S_{tr}}{\tau_1} e^{-(t-t_0)/\tau_1} \int_{t_0}^{t} e^{t'/\tau_1} \Delta F(t' - t_0) dt' \quad \text{(S9.5)}$$

In the following, the time of cessation of emissions t_0 is set equal to zero, with forcing and temperature change expressed relative to their values at that time, as a function of time t subsequent to the time of cessation:

$$\Delta T(t) = \frac{S_{tr}}{\tau_s} e^{-t/\tau_s} \int_{0}^{t} e^{t'/\tau_s} \Delta F(t') dt' + \frac{S_{eq} - S_{tr}}{\tau_1} e^{-t/\tau_1} \int_{0}^{t} e^{t'/\tau_1} \Delta F(t') dt' \quad \text{(S9.6)}$$

The change in forcing due to abrupt cessation of emissions associated with fossil fuel combustion, consists of contributions arising from change in forcing by CO_2 and by combustion-derived aerosols

$$\Delta F_{tot} = \Delta F_{CO2} + \Delta F_{aer} \quad \text{(S9.7)}$$

Because of the linearity of the system represented in Eq (2) the responses to these forcings may be calculated individually and then summed to obtain the total response. On account of the short atmospheric residence time of combustion-derived aerosols the change in forcing by aerosols is taken as equal to the negative of the aerosol forcing at time of cessation of emissions,

$$\Delta F_{aer} = -F_{aer}^{0}, \quad \text{(S9.8)}$$

a step-function positive forcing at time 0, the cessation of a negative forcing being a positive forcing. The changes in temperature are calculated for the high, best-estimate, and low magnitude aerosol forcing; on account of the tight coupling between S_{tr} and F^0_{aer} (Figure 2*b*) the appropriate value of S_{tr} must be used for a given value of F^0_{aer}.

As shown in SI §S6, the change forcing by CO_2 that would result from the decrease in excess CO_2 subsequent to cessation of emissions is well approximated as linear in the change in mixing ratio.

$$\Delta F_{CO2}(t) = \beta\{[CO_2](t) - [CO_2]_0\} \tag{S9.9}$$

In the following the change in mixing ratio is represented as an exponential decrease of excess CO_2 above preindustrial (pi) with time t subsequent to cessation of emissions;

$$[CO_2](t) = [CO_2]_{pi} + ([CO_2]_0 - [CO_2]_{pi})e^{-t/\tau_{CO2}}. \tag{S9.10}$$

As τ_{CO2} is quite uncertain, the change in forcing due to the decrease in CO_2 is examined for a set of time constants within the uncertainty range. For forcing linear in $\Delta[CO_2]$, the time dependent forcing is

$$\Delta F_{CO2} = \beta([CO_2]_0 - [CO_2]_{pi})(1 - e^{-t/\tau_{CO2}}) \tag{S9.11}$$

Convolution with the exponential decay function for climate system response (Eq S9.11) yields an expression for the change in GMST as a function of time subsequent to cessation of emissions

$$\Delta T(t) = -S_{tr}F^0_{aer}\left[1 - e^{-t/\tau_s}\right] - S_{tr}F^0_{CO2}\left(\left[1 - e^{-t/\tau_s}\right] - \left(\frac{\tau_{CO2}}{\tau_{CO2} - \tau_s}\right)\left[e^{-t/\tau_{CO2}} - e^{-t/\tau_s}\right]\right)$$
$$-(S_{eq} - S_{tr})F^0_{aer}\left[1 - e^{-t/\tau_1}\right] - (S_{eq} - S_{tr})F^0_{CO2}\left(\left[1 - e^{-t/\tau_1}\right] - \left(\frac{\tau_{CO2}}{\tau_1 - \tau_{CO2}}\right)\left[e^{-t/\tau_1} - e^{-t/\tau_{CO2}}\right]\right) \tag{S9.12}$$

that may be readily evaluated for a suitable set of values of S_{tr}, S_{eq}, F^0_{aer}, τ_s, τ_1, and τ_{CO2}, Figure 5; Figure S6. Alternatively, of course, the temperature response to any arbitrary forcing function can be obtained by numerical integration, but the analytical expression provides much insight. In particular the analytical expression permits determination of the time, subsequent to cessation of emissions, t_{max}, of occurrence of the maximum increase in temperature ΔT_{max} within the assumption that the cessation of sources occurs for the system at quasi steady state and for the approximation that heat uptake into the lower compartment is neglected (first line of Eq S9.12). The resulting expression for t_{max}

$$t_{max} = \frac{\tau_s\tau_{CO2}}{\tau_{CO2} - \tau_s}\ln\left[\frac{-F^0_{aer}}{F^0_{CO2}}\frac{\tau_{CO2} - \tau_s}{\tau_s}\left(1 + \frac{\tau_s}{\tau_{CO2} - \tau_s}\frac{F^0_{CO2}}{-F^0_{aer}}\right)\right], \tag{S9.13}$$

depends on F^0_{aer}, τ_s and τ_{CO2} but does not depend on climate sensitivity. The maximum increase in GMST that would be experienced subsequent to an abrupt cessation in emissions, ΔT_{max}, is readily evaluated by Eq S9.12 for $t = t_{max}$, as a function of F^0_{aer} for specified values of τ_s and τ_{CO2}; (as anticipated, the effect of the second line of Eq S9.12 on t_{max} and ΔT_{max} is negligible). These quantities are shown in Figure S7. Here the independent variable taken as the magnitude of aerosol forcing at the time of cessation F^0_{aer}; the implicit dependence of ΔT_{max} on S_{tr} is accounted for through the dependence of S_{tr} on F^0_{aer} shown in Figure 2*b*. For the best-estimate aerosol forcing magnitude 0.9 W m^{-2}, t_{max} ranges from about 10 to 30 years, depending mainly on the adjustment time of excess CO_2 τ_{CO2}, a shorter adjustment time resulting in a lower value of t_{max} and vice versa. Likewise t_{max} is shorter for lower values of τ_s. For the entire range of variables examined t_{max} is less than about 30 years, after which time the effect of decrease in forcing by CO_2 increasingly offsets the step function increase in forcing due to cessation of aerosol forcing, as seen also in the time dependence of ΔT shown in Figures 5, supporting the focus of the present calculations on the initial decades following cessation of emissions. For any given value of F^0_{aer} the values of ΔT_{max} are tightly bundled, Figure S7*b*, exhibiting the expected strong dependence on aerosol forcing (and implicitly on climate sensitivity) but with only slight dependence on τ_{CO2} and even less on τ_s, the range of values for any given F^0_{aer} not exceeding more than about 0.2 K. Indeed the values of ΔT_{max} are within about 0.2 K of $\Delta T_{inst,aer}$, the increase in GMST that would be exhibited if the response of the climate system to the cessation of aerosol forcing were instantaneous and there were no decrease in GMST due to decrease in CO_2 forcing. As this quantity, shown also in Figures 2*b* and 5*b*, is readily evaluated without consideration of the time dependence of decrease of CO_2 forcing and climate system response to forcing, it serves as a convenient and accurate estimator of the increase in GMST that would occur in response to abrupt cessation of anthropogenic aerosol forcing.

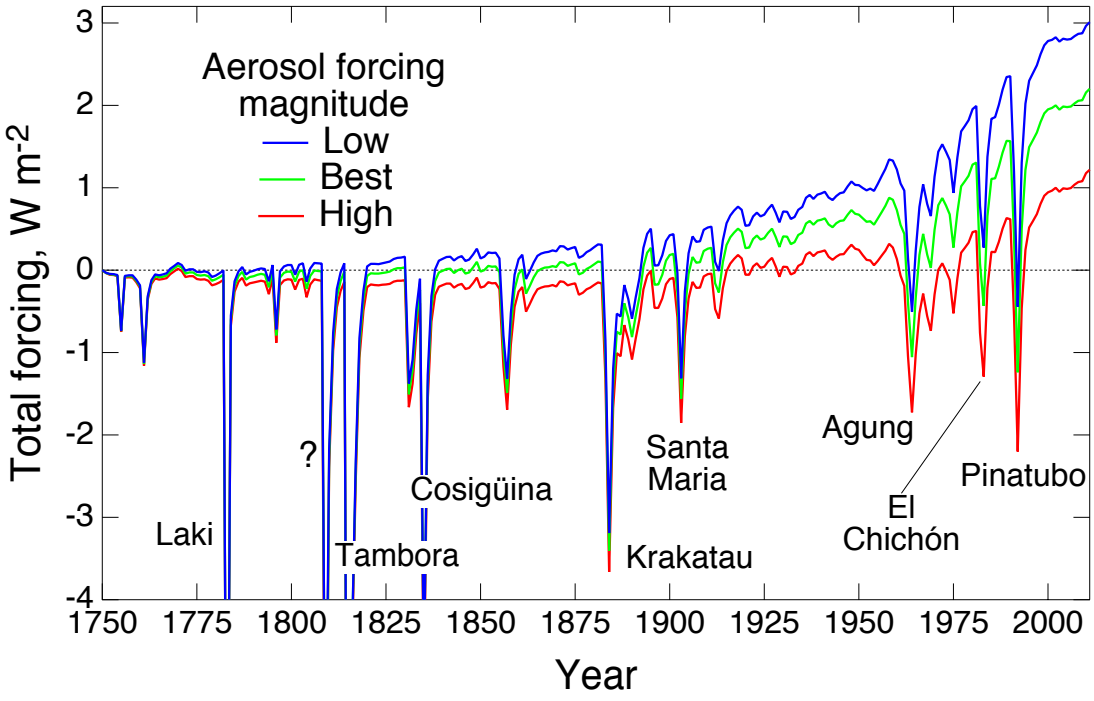

Figure S1. Time series of estimated global-mean total forcing relative to 1750, for best estimate of this forcing F_{aB} (green) and for forcing by anthropogenic aerosols scaled by the 5% (low, blue) and 95% (high, red) limits of the uncertainty range given by IPCC AR5 for this forcing in 2011, F_{aH} and F_{aL}, respectively. Short-duration negative spikes in forcing are estimates of forcing by stratospheric aerosols resulting from impulsive volcanic eruptions (identified in figure). Data are from Supporting Information to Chapter 8, Annex II: Climate System Scenario Tables, Table AII.1.2, "Historical effective radiative forcing (ERF) (W m^{-2}), including land use change (LUC)" (Prather *et al.*, 2013).

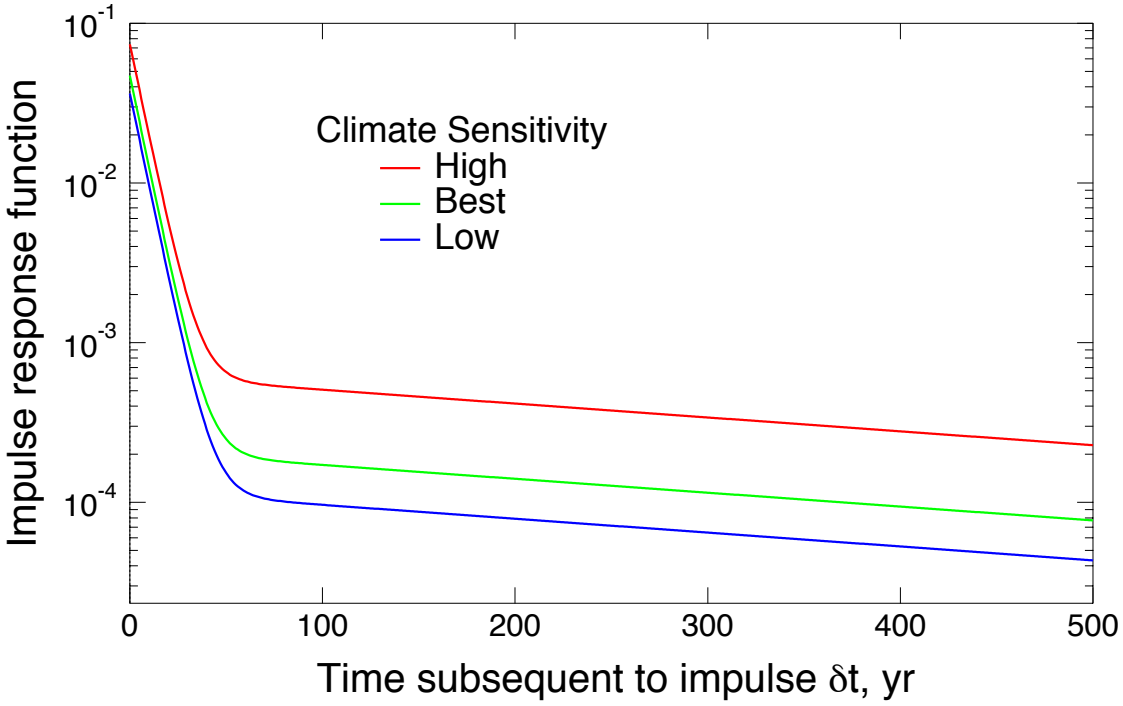

Figure S2. Impulse functions relating change in GMST at time $t + \delta t$, due to unit forcing at time t, as determined and used in this study for high, best-estimate, and low values of climate sensitivity.

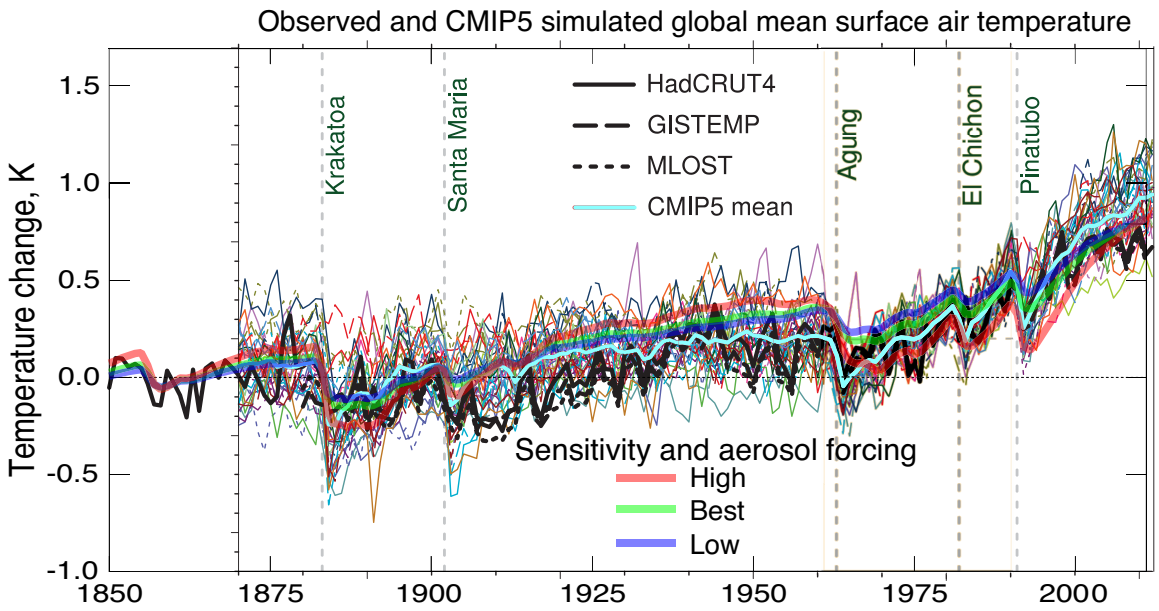

Figure S3. Time series of change in global temperature (relative to 1850-1900) obtained by convolution of time series of total forcing for high, best-estimate, and low climate sensitivity and aerosol forcing with corresponding impulse response functions, superimposed on Figure 9.8*a* of Flato *et al*. (2013). That figure presented time series for change in GMST calculated by 36 climate models that participated in the Coupled Model Intercomparison Project Phase 5 (CMIP5), shown by thin lines, together with the multi-model mean and three time series for GMST reconstructed from observations: HadCRUT4 (Hadley Center and Climatic Research Unit), GISTEMP (Goddard Institute for Space Studies) and MLOST (Merged Land–Ocean Surface Temperature analysis). Also shown are dates of major impulsive volcanic eruptions. For identification of individual models and citations see Flato *et al*. (2013).

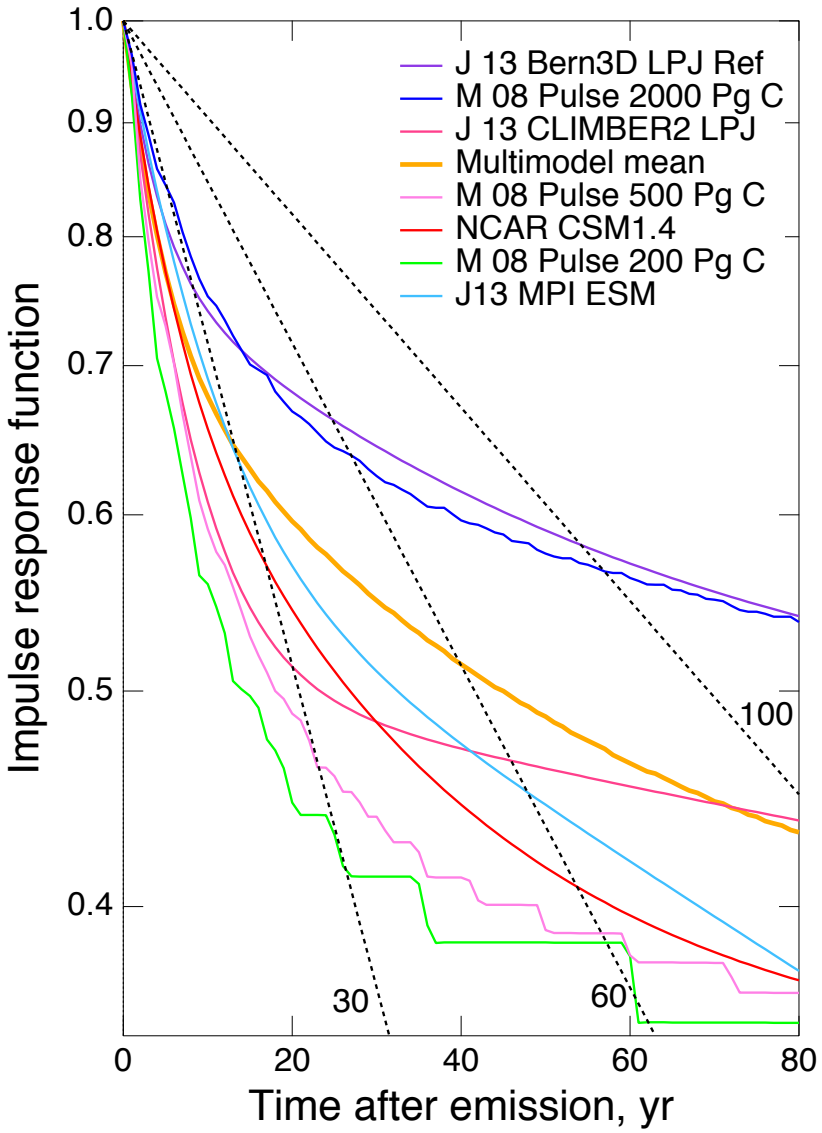

Figure S4. Impulse response functions IRFs employed in convolution with CO_2 emissions. IRF denotes fraction of pulse emission at time t_0 remaining in atmosphere as a function of time subsequent to emission. Sources of IRFs are as in Figure 3 and Table 2. Also shown exponential decay curves (straight lines on the semilogarithmic plot) with indicated time constants. Jags in curves results from digitization of published figures.

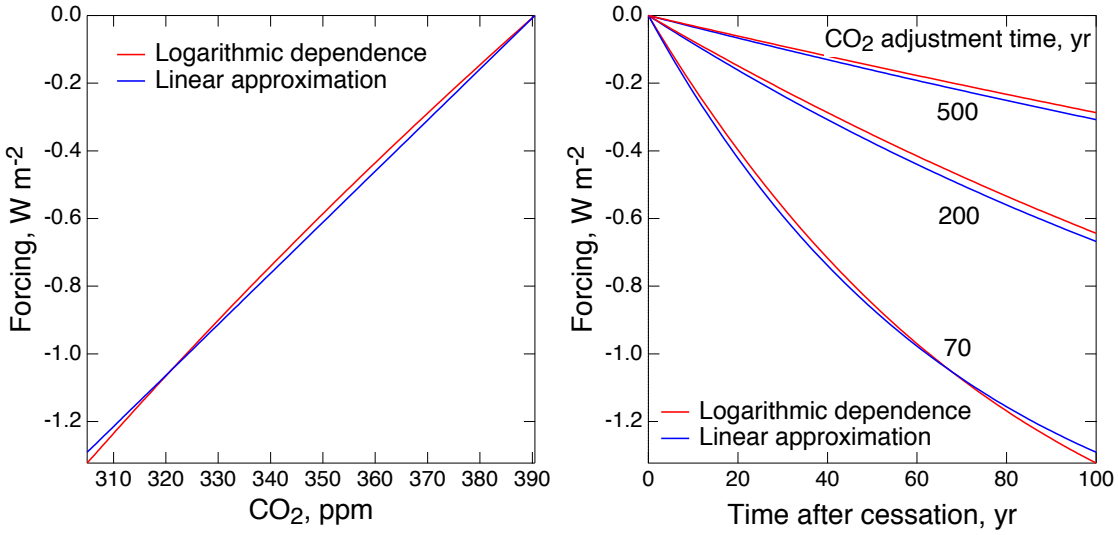

Figure S5. Dependence of forcing by CO_2 on decrease in CO_2 from initial value, 390.5 ppm, at time of cessation of emissions as function of CO_2 mixing ratio, *a*, and time after cessation of emissions, *b*, for forcing represented as logarithm of CO_2 mixing ratio, red, and by linear approximation. Here $\beta = 0.0151$ W m^{-2} ppm^{-1}. Time dependent decrease of CO_2 mixing ratio and forcing is calculated for indicated values of adjustment time τ_{CO2}, the time constant for decrease of excess CO_2 above preindustrial value 278 ppm to 1/*e* of its initial value in the absence of emissions.

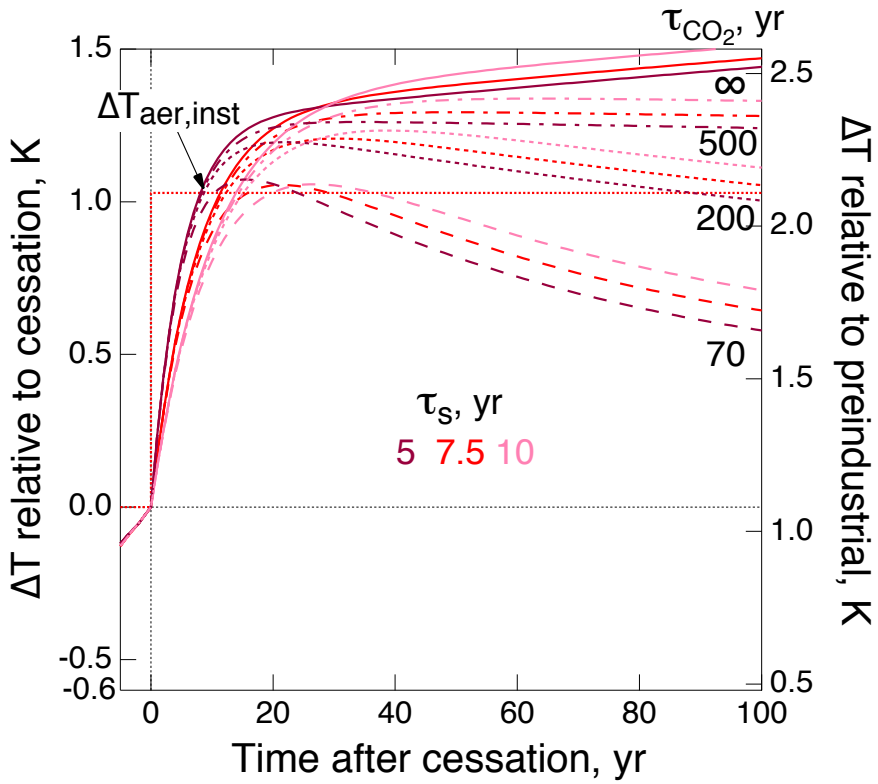

Figure S6. Global temperature response (solid curves) following abrupt cessation of sources of CO_2 and aerosols for the high-sensitivity, high-magnitude aerosol forcing case examined in Figure 5. Time constant of upper compartment of climate system τ_s was taken as 5, 7.5, and 10 yr. Curves are shown for adjustment time of excess CO_2 above preindustrial τ_{CO2} = 70, 200, and 500 years and constant CO_2, ($\tau_{CO2} = \infty$). Also shown, right axis, are the increases in GMST above preindustrial, as in Figure 5.

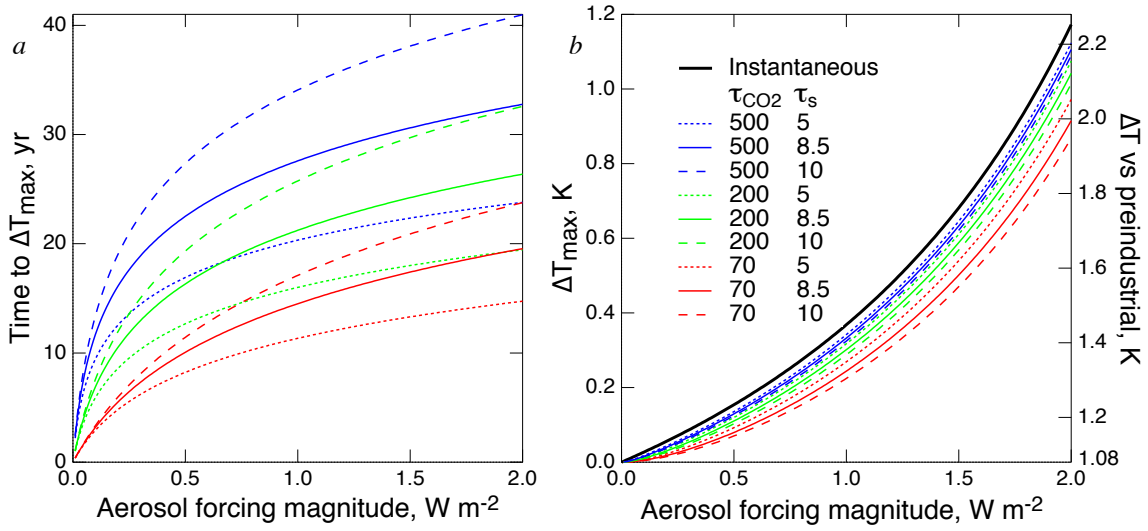

Figure S7. *a*, Time to reach maximum increase in GMST and *b*, maximum increase in GMST, relative to value at time of cessation (left axis) following abrupt cessation of emissions, as function of magnitude of aerosol forcing at time of cessation, for indicated values of adjustment time of excess CO_2 τ_{CO2} and time constant of upper compartment of the climate system τ_s. Also shown, *b*, right axis, are the increases in GMST relative to preindustrial, as in Figure 5.

Aerosol forcing magnitude	F_{tot} wrt 1850–1900	$S_{tr,u}$	dF/dt	$\Delta T_{unrealized}$, K			S_{tr},
	W m^{-2}	K/(W m^{-2})	W m^{-2} yr^{-1}	τ_s = 5 yr	τ_s =7.5 yr	τ_s = 10 yr	K/(Wm^{-2})
High	1.7	0.5	0.023	0.058	0.086	0.12	0.55 ±0.02
Best	2.44	0.33	0.021	0.035	0.052	0.069	0.35 ±0.01
Low	3.05	0.26	0.019	0.025	0.037	0.049	0.27 ±0.01

Table S1. Estimation of unrealized temperature increase. Transient sensitivity parameter S_{tr} and rate of change of forcing dF/dt, are from Figure 1 for the three time series of estimated total forcing. Unrealized warming is with respect to quasi–steady-state temperature increase evaluated with the transient sensitivity, not with respect to the long-time temperature increase given by the equilibrium sensitivity.

Data Set S1. Forcing and temperature change, Figures 1, S1, S3.

Data Set S2. CO_2 Impulse response functions, Figure S3.

Data Set S3. CO_2 emission rates, used in convolutions shown in Figure 3.

Data Set S4. Fractional excess atmospheric CO_2 as function of time after cessation of emissions, Figure 3.

Data Set S5. Forcing by CO_2 as function of time subsequent to cessation of emissions, Figure 4*a*.

Data Set S6. Change in GMST in response to cessation of sources as function of time subsequent to cessation, Figures 5, S6.

Data Set S7. Time to reach maximum increase in GMST and magnitude of maximum increase in GMST subsequent to cessation of sources as function of aerosol forcing, Figure S7.